IEEE Access
Multidisciplinary | Rapid Review | Open Access Journal

SPECIAL SECTION ON RECENT ADVANCES ON RADIO ACCESS AND SECURITY METHODS IN 5G NETWORKS

Received October 11, 2017, accepted November 6, 2017, date of publication November 21, 2017,
date of current version February 14, 2018.

Digital Object Identifier 10.1109/ACCESS.2017.2776145

RF Compliance Study of Temperature Elevation in Human Head Model Around 28 GHz for 5G User Equipment Application: Simulation Analysis

WANG HE[1], BO XU[1,2], (Student Member, IEEE), MATS GUSTAFSSON[3], (Senior Member, IEEE), ZHINONG YING[4], (Senior Member, IEEE), AND SAILING HE[1,2], (Fellow, IEEE)

[1]Zhejiang Provincial Key Laboratory for Sensing Technologies, Centre for Optical and Electromagnetic Research, Zhejiang University, Hangzhou 310058, China
[2]Department of Electromagnetic Engineering, KTH Royal Institute of Technology, SE-100 44 Stockholm, Sweden
[3]Department of Electrical and Information Technology, Lund University, SE-221 00 Lund, Sweden
[4]Network Technology Laboratory, Research and Technology, Sony Mobile Communications AB, SE-221 88 Lund, Sweden

Corresponding author: Sailing He (sailing@jorcep.org)

This work was supported in part by the Program of Zhejiang Leading Team of Science and Technology Innovation under Grant 2010R50007, in part by Swedish VR, in part by AOARD, in part by Fundamental Research Funds for Central Universities, and in part by the China Scholarship Council under Grant 201506320137.

ABSTRACT The crowdedness of current cellular bands and the demand for higher transmission speed prompt the use of the millimeter-wave spectrum for the next-generation mobile communication. In the millimeter-wave frequencies, the dosimetric quantity for human exposure to electromagnetic fields changes from the specific absorption rate to incident power density. In this paper, we used 28-GHz beam-steering patch arrays, a dipole antenna, and plane waves to investigate the temperature elevation in a multi-layer model of human head and its correlation with power density metrics. The power density averaged over one square-centimeter in free space and the peak temperature elevation in tissue at 28 GHz have good correlation. The peak temperature elevation indicated by the power density averaged one square-centimeter also agrees well with the peak temperature elevation induced by the plane waves. The results show that the averaging area of a few square-centimeters may be a good candidate for the spatial-average power density. The findings provide valuable input to the ongoing revision and updating of relevant safety standards and guidelines.

INDEX TERMS 28 GHz, 5G, antenna array, human head, incident power density, millimeter wave, RF compliance, safety guidelines, safety standards, temperature elevation, user equipment.

I. INTRODUCTION

As the frequency bands below 6 GHz are currently very crowded, increasing demands for greater channel capacity and higher data rates have prompted exploration of the millimeter-wave (mmWave) spectrum towards the next-generation (5G) mobile communication [1], [2]. One of the mmWave bands allocated towards 5G in 2016 by the U.S. Federal Communications Commission (FCC) is located around 28 GHz [3], which is expected for the first 5G commercial products by 2020. However, the path loss also drastically grows in the mmWave frequencies due to the downsizing of antenna dimensions [4] and increasing atmospheric absorption [5]. One solution to compensate for the higher loss is to deploy antenna arrays in 5G base stations and user equipment (UE) [6]–[10]. Array antennas not only provide extra array gain, but also enable beam scanning by controlling the phase excitation of each element.

However, the technical feasibility of mmWave communications also leads to safety concerns that the exposure to mmWave electromagnetic fields (EMFs) may cause adverse health effects on the general public. EMF exposure limits in the radio frequencies (RF), including the mmWave bands, are established to prevent from excessive tissue heating, which can cause thermal pain and burns. Usually, it requires about 10 °C above the skin temperature in an ordinary room environment to feel thermal pain or to be burned when reaching the threshold temperature for minutes [11]. According to the International Commission on Non-Ionizing Radiation Protection (ICNIRP) [12] and the IEEE guidelines [13] regarding RF EMF exposure, a 1 °C rise in temperature,

TABLE 1. Regulatory power density limits for the general public below 100 GHz.

	ICNIRP		IEEE				FCC (present)	FCC (proposed)
frequency range (GHz)	≥ 10		3–30		30–100		≥ 6	
power density limits (W/m^2)	10	200	10	$18.56f^{0.699}$	10	200	10	
peak/averaging area (cm^2)	20	1	$100\lambda^2$	spatial peak	100	spatial peak	spatial peak	1
averaging time (min)	$(68/f^{1.05})$[b]		$150/f$		$25.24/f^{0.476}$		30	

even in the most sensitive tissues and organs, is not adverse.[a] To protect from excessive heating generated by the existent 2G–4G UE, the exposure limits are expressed as the specific absorption rate (SAR) averaged over 10 g of tissue below 3 GHz and 10 GHz for the IEEE and the ICNIRP, respectively, and averaged over 1 g of tissue below 6 GHz for the FCC [12]–[15]. Below these frequencies, the correlation between SAR and the temperature elevation in tissue, ΔT, is stable, and the SAR measurement has been widely applied for the evaluation of RF exposure of 2G–4G cellular UE [16]–[27]. However, above these frequencies, the energy penetration depth becomes shallow (e.g., less than 2 mm at 15 GHz and less than 1 mm at 30 GHz) and the correlation between SAR and ΔT becomes weak [28]. Thus, incident power density replaces SAR in the safety guidelines and standards above 3 GHz–10 GHz. Between 3 GHz and 6 GHz, the IEEE allows one to evaluate RF EMF exposure with either SAR or power density.

Recently, many efforts have been made to evaluate mmWave exposure and RF compliance for 5G. References [29]–[31] studied the maximum permissible transmitted power complying with different regulatory power density limits from 5G array antennas in terms of frequencies, array topology, array size, and the number of array elements. References [32]–[34] investigated different methods dealing with SAR, power density assessment, and measurement for mmWave array antennas. References [35]–[39] conducted a series of thermal modeling studies for 5G mmWave exposure.

However, some literature [29]–[33] only considered the RF compliance from the perspective of mmWave antenna design without taking ΔT into account, while other studies [35]–[39] considered the RF compliance from the perspective of thermal modeling techniques without considering realistic antenna design. Thus, one motivation of this study is to bridge the gap between the previous mmWave antenna studies and thermal modeling studies. Additionally, [29]–[32] showed that the incident power density levels of an array antenna at 1 mm can be higher than those at 10 mm by tenfold, while [36]–[39] placed antennas at least 15 mm away from tissue, which may not be the worst case scenario that leads to the highest ΔT. Thus, the other motivation is to examine whether the peak ΔT shows a high increase under near-field exposure.

[a]The IEEE guidelines state that "More recent WHO information indicates that a 1 °C rise in temperature, even in the most sensitive tissues and organs, is not adverse." The ICNIRP Guidelines state that "Many laboratory studies with rodent and non-human primate models have demonstrated the broad range of tissue damage resulting from either partial-body or whole-body heating producing temperature rises in excess of 1 − 2 °C."

The near-field exposure in this study is produced by a 2 × 2 beam-steering patch array, a 4 × 1 fixed-beam patch array, and an 8 × 1 fixed-beam patch array. The antennas are placed from 1 mm up to 20 mm above the head model. A dipole antenna and a plane-wave source are used as references for benchmarking. The correlations between ΔT and incident power density complying with different guidelines and standards are provided, which are of particular interest for 5G RF compliance research. As the guidelines and standards for 5G EMF exposure are in the process of revision and updating, this study can provide valuable input.

II. DOSIMETRY, MODELS, AND METHODS

A. THERMAL DOSIMETRY

The temperature in human tissue can be modeled by Pennes's bioheat transfer equation (BHTE) [40]:

$$C(\boldsymbol{r})\,\rho(\boldsymbol{r})\,\frac{\partial T(\boldsymbol{r},t)}{\partial t} = \nabla\cdot\left(K(\boldsymbol{r})\,\nabla T(\boldsymbol{r},t)\right) + \rho(\boldsymbol{r})\,SAR(\boldsymbol{r}) + Q(\boldsymbol{r},t) - B(\boldsymbol{r},t)\left(T(\boldsymbol{r},t) - T_{\mathrm{B}}(\boldsymbol{r},t)\right), \quad (1)$$

where T is the temperature of the tissue; T_{B} is the blood temperature; C is the specific heat of tissue; K is the thermal conductivity of tissue; Q is the metabolic heat generation; B represents the blood perfusion; $\boldsymbol{r}$ and t denote the position vector and time, respectively; and SAR is calculated by

$$SAR(\boldsymbol{r}) = \frac{\sigma(\boldsymbol{r})}{\rho(\boldsymbol{r})}|E_{\mathrm{ind}}(\boldsymbol{r})|^2, \quad (2)$$

in which $\boldsymbol{E}_{\mathrm{ind}}$ is the root-mean-square induced electric field in tissue, and σ and ρ are the electrical conductivity and the mass density of tissue, respectively. The boundary condition at the interface between air and skin for BHTE is expressed as

$$-K(\boldsymbol{r})\,\frac{\partial T(\boldsymbol{r},t)}{\partial n} = H\cdot\left(T_{\mathrm{S}}(\boldsymbol{r},t) - T_{\mathrm{e}}(t)\right), \quad (3)$$

where H, T_{S}, and T_{e} are the heat transfer coefficient of the interface, the temperature of the skin surface, and the temperature of air, respectively.

The regulatory guidelines and standards require that incident power density should be averaged over a certain period of time. As shown in Table 1, the averaging time at 28 GHz is about 2 minutes [12], 5 minutes [13], and 30 minutes [15] for the ICNIRP, the IEEE, and the FCC, respectively, although the averaging time in the guidelines and standards refers

[b]In Table 1, f is the frequency in GHz. For example, at 28 GHz, $68/f^{1.05} = 68/28^{1.05} \approx 2$ (min).

TABLE 2. Parameters of multi-layer head model.

	tissue	thickness (mm)	ε_r	σ (S/m)	K (W/K/m)	B (W/K/m^3)	ρ (kg/m^3)
a	skin	1.5	18.71	26.19	0.42	9100	1100
b	fat	1.5	3.70	1.70	0.25	520	916
c	muscle	2.5	24.44	33.61	0.50	2700	1041
d	skull	4.5	7.51	8.88	0.40	1000	1990
e	dura	1.0	19.50	24.74	0.50	2700	1130
f	cerebrospinal fluid	1.0	28.19	43.80	0.60	0	1007
g	brain	4.0	18.59	25.86	0.54	35000	1041

to incident power density at present, not thermal modeling. Under constant exposure, it takes about 10–15 minutes for the temperature to reach the steady state [37], which is considered in this study for the conservative evaluation of ΔT. The blood temperature, T_B, can be treated as constant because the exposure scenario considered here is localized. The absorption of power radiated by UE is much smaller than the metabolic heat generation of a male adult, thus the metabolic heat generation Q can be ignored [36]–[38]. For the steady state, the term at the left side of (1) is zero, and other terms are independent of time, thus the steady-state BHTE can be written as

$$\nabla\cdot(K(\boldsymbol{r})\nabla T(\boldsymbol{r}))+\rho(\boldsymbol{r})SAR(\boldsymbol{r})-B(\boldsymbol{r})(T(\boldsymbol{r})-T_B)=0. \tag{4}$$

The temperature elevation, ΔT, can be calculated via the temperature distribution in (4) with and without EMF sources.

B. INCIDENT POWER DENSITY

Incident power density, i.e., the free space Poynting vector, is the regulatory dosimetric quantity for the frequencies listed in Table 1. The FCC at present stipulates that the spatial-peak power density should not exceed 10 W/m^2, and proposed to use 1 cm^2 averaged power density to replace the spatial-peak condition has not yet been adopted [41], [42]. In this study, they are referred as the 'present' and 'proposed' FCC limits. The ICNIRP stipulates that the power density should not exceed 10 W/m^2 averaged over any 20 cm^2 and should not exceed 200 W/m^2 over any 1 cm^2 [12]. The IEEE stipulates that the power density averaged over $100\lambda^2$ for frequencies from 3 to 30 GHz, i.e. approximately 114 cm^2 at 28 GHz, should not exceed 10 W/m^2 [13], [14]. A brief summary of the power density limits is listed in Table 1.

Incident power density of antennas averaged over an area, A, as shown in Fig. 1, can be expressed as

$$S^{av}=\frac{1}{2A}\int_A \mathrm{Re}(\boldsymbol{E}_{FS}\times\boldsymbol{H}^*_{FS})\cdot\hat{\boldsymbol{n}}\,dA, \tag{5}$$

where the superscript $*$ denotes the complex conjugate, $\boldsymbol{E}_{FS}$ and $\boldsymbol{H}_{FS}$ are the electric and magnetic fields in free space, respectively, $\hat{\boldsymbol{n}}$ denotes the unit vector normal to A. For the proposed FCC limits, $A = 1$ cm^2; for the ICNIRP limits, $A = 20$ cm^2 or 1 cm^2; and for the IEEE limits, $A \approx 114$ cm^2 at 28 GHz. We assume that the area A is square-shaped here.

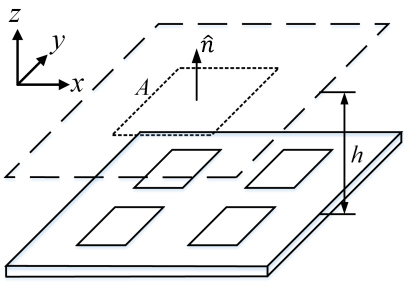

FIGURE 1. The diagram of the spatial-average power density.

The spatial-peak power density is not well defined in the guidelines and standards, and could be interoperated in two ways [43]. Considering $A \to 0$ in (5), the spatial-peak power density can be written as the Poynting vector projected in the $\hat{n}$-direction (e.g., [32]), which is stated by the International Electrotechnical Commission (IEC) TC106 AHG10:

$$S^p_n=\frac{1}{2}\mathrm{Re}\left(\boldsymbol{E}_{FS}\times\boldsymbol{H}^*_{FS}\right)\cdot\hat{\boldsymbol{n}} \tag{6}$$

The spatial-peak power density can also be written as the magnitude of the Poynting vector, which might be required by some regulators thus is also of interest:

$$S^p=\frac{1}{2}\left|\mathrm{Re}\left(\boldsymbol{E}_{FS}\times\boldsymbol{H}^*_{FS}\right)\right| \tag{7}$$

Here, we adopt the latter expression (7), as it gives higher power density values than (6), and thus it is more conservative for the maximum permissible transmitted power [43]. Nevertheless, choosing either (6) or (7) has neglegible impact on the conclusion of this paper.

C. MULTI-LAYER HUMAN HEAD MODEL

To facilitate the calculation of BHTE, human heads can be approximated using the multi-layer model [36]–[38], as shown in Fig. 2(a) and Table 2. The length and the width of the model, i.e. w, is set to 60 mm. As long as w is large compared to the size of the thermal hot spot caused by the illuminating EMFs, the accuracy of ΔT should be acceptable. The dielectric parameters of tissue at 28 GHz come from a four-Cole-Cole dispersion model [36]–[38], [45]. The thermal parameters of tissue are available in [46]. The separation distance between antennas and the head model is denoted h.

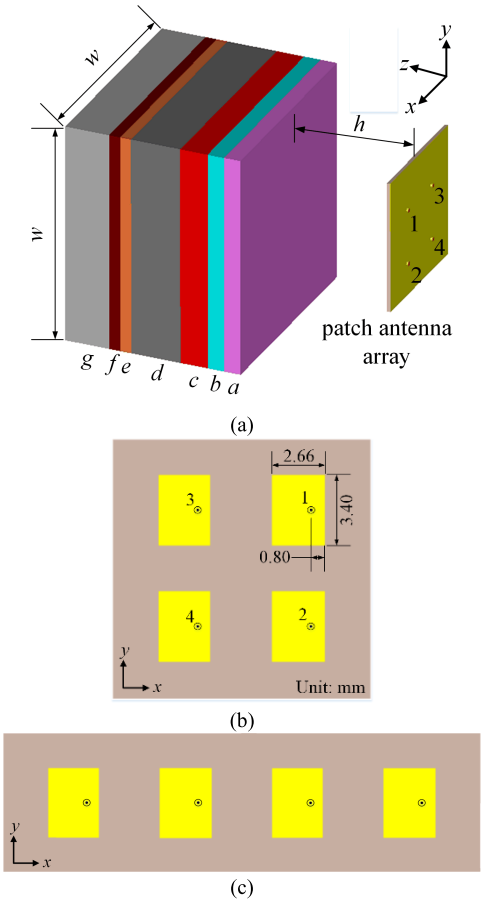

FIGURE 2. (a) Exposure scenario with the multi-layer head model, the parameters of which are shown in Table 2, and the top view of (b) the 2 × 2 patch antenna array and (c) the 4 × 1 patch antenna array. The 8 × 1 patch array is not shown in the figure for simplicity, but has the same orientation and element spacing as the 4 × 1 patch antenna array.

D. ANTENNA MODELS

To realize full-spherical coverage for 5G UE, the array configurations with an 8×1 array, two 4×1 or 2×2 subarrays are proposed in 3GPP [47]. A 2 × 2 beam-steering patch array, a 4 × 1 and an 8 × 1 fixed-beam patch array, together with a half-wavelength dipole and plane waves, are considered as EMF sources in this study. Fig. 2(b) shows the layout of the coaxial-fed 2 × 2 patch array whose element spacing is equal to half a wavelength, i.e., 5.36 mm. The thickness, the relative permittivity, and the loss tangent of the substrate are 0.3 mm, 3.38, and 0.0027, respectively. The phase difference, $\Delta\phi$, is chosen as 0°, 60°, and 120° between ports 1 and 2 and ports 3 and 4, as shown in Table 3, thus the main beam can be steered from boresight to about 30° in the E-plane, as shown in Fig. 3. The 4 × 1 patch array shown in Fig. 2(c) has the same element design and element spacing as the 2 × 2 patch array, but only the in-phase exaction is considered with a fixed beam in the boresight direction. The 8 × 1 patch array is not shown in the figure for simplicity, but has the same orientation and element spacing as the 4 × 1 patch antenna array. The half-wavelength dipole is placed along the y-direction.

TABLE 3. Phase shift angles for the 2 × 2 patch antenna array.

No.	Port 1	Port 2	Port 3	Port 4
1	0°	0°	0°	0°
2	0°	0°	60°	60°
3	0°	0°	120°	120°

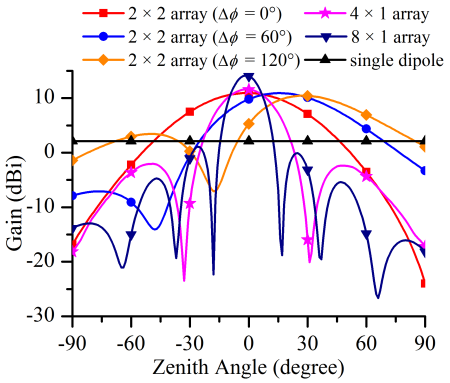

FIGURE 3. The E-plane pattern of the 2 × 2 patch antenna array with $\Delta\phi = 0°$, 60°, and 120°, the 4 × 1 and 8 × 1 patch antenna arrays and a single dipole.

The propagation direction of the plane wave is perpendicular to the skin.

E. SIMULATION SET-UP

The commercial simulation software CST [48] is used for full-wave simulations in this study. The electromagnetic problem is solved by the CST high-frequency electromagnetic package MWS and the resulting SAR distribution is used as the thermal source coupled into the CST multi-physics package MPS. The same model is shared in MWS and MPS. In MWS, using the time-domain solver based on the Finite Integration Technique (FIT), the boundary conditions are all set to be perfectly match layers (PMLs). In MPS, using the thermal steady-state solver based on (3) and (4), the boundaries normal to the x- and y-axes are set to be adiabatic, the boundary in the $-z$-direction is set to be isothermal with temperature equal to that of the core body, 37°, and the boundary in the $+z$-direction at infinity set to be the room temperature of 23 °C. w should be large enough such that the adiabatic boundary condition would hardly affect the peak ΔT around the center of the skin layer, as to be shown below. The heat transfer coefficient H is set to $5\text{W}/(\text{m}^2\cdot{}^\circ\text{C})$ at the interface between the air and the skin [49], [50].

The maximum permissible transmitted power of mmWave antennas complying with the present regulatory guidelines are far below the transmitted power levels of current 2G–4G UE (23 dBm–33 dBm) [29], [30], [39]. For the ICNIRP, assuming all power flows across 20 cm^2 in an extreme situation, the transmitted power should be 13 dBm [30]. The maximum permissible transmitted power of a dipole antenna above 6 GHz complying with the present FCC

limits is about 15 dBm [29], [39]. In this study, the total input power levels for all antennas are set to 15 dBm, which is a reasonable estimate for 28 GHz.

III. RESULTS

A. VALIDATION OF MODEL SIZE

To ensure that w is large enough for simulation, the peak ΔT is computed for different w with the 2×2 patch array and the separation distance $h = 20$ mm. As shown in Fig. 4, the peak ΔT reaches steady convergence when $w \geq 60$ mm, thus choosing the length and the width of the model as $w = 60$ mm has limited effects on the peak ΔT.

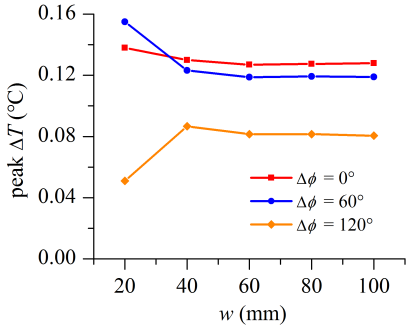

FIGURE 4. The peak ΔT on the multi-layer model with different w, induced by a 2 × 2 patch array with $\Delta\phi = 0°$, 60°, and 120°.

B. ANTENNA CHARACTERISTICS

All the antennas in this study are resonant at $f_c = 28$ GHz in free space. When the antennas are placed close to the head model, the antenna input impedance changes. For conservative evaluation of the peak ΔT, we selected different best matching frequencies, f_m, rather than f_c, for different h. As shown in Fig. 5, f_m is where the total accepted power of antennas, P_a, reaches a maximum, P_{am}. P_{am} probably, though not necessarily, leads to the largest SAR. It can be seen in Fig. 6 that f_m fluctuates, especially for $h \leq 10$mm. In practice, the mobile communication system works not at a single frequency point, but within some bands. Therefore, it is reasonable to use f_m and P_{am} for the conservative evaluation of the peak ΔT, instead of using f_c and its corresponding total accepted power, P_{ac}.

C. TEMPERATURE ELEVATION

Fig. 7(a) shows the hot spots on the skin surface. An interesting feature is that the hot spot moves with the scan angle; meanwhile, the corresponding ΔT decreases. This is because the electric field, with a larger scan angle, is likely easier to be reflected than that with smaller angle [28] and the tilted beam has a greater illuminating area. Fig. 7(b) shows the cross sections of the ΔT distributions of the 2×2 patch array with $\Delta\phi = 0°$ and the dipole at $h = 1$ mm and 10 mm. It can be seen that heating is mainly localized in the skin and fat layers. The peak ΔT caused by the arrays, on one hand, is lower than the peak ΔT of the dipole at $h = 1$ mm and on the other

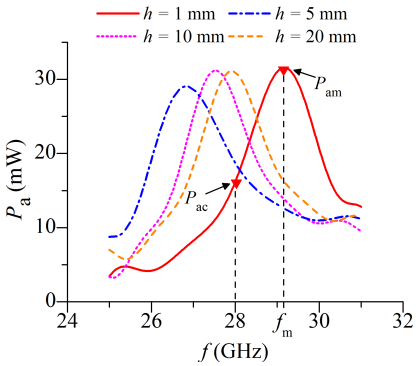

FIGURE 5. The accepted power P_a of the 2 × 2 patch antenna array with $\Delta\phi = 0°$ and $h = 1$, 5, 10, and 20 mm.

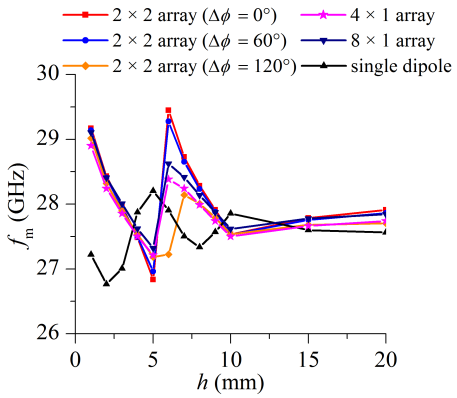

FIGURE 6. f_m versus h for different antennas.

hand, is higher than the peak ΔT of the dipole at $h = 10$ mm. This phenomenon originates from the fact at a very close distance, the radiated power of a single dipole is concentrated in a much smaller space than that of an array. As shown in Fig. 7(b), the diameters of the hot spot areas with $\Delta T \geq 1$ °C are 12.3 mm and 10.1 mm at $h = 1$ mm for the array and the dipole, respectively. At the farther distance, the ΔT of the dipole is lower than the ΔT of the array due to the energy focusing of the array.

Fig. 8 shows the peak ΔT changing with h for different antennas. Generally, the peak ΔT decreases with increasing h. For the 2×2 array, the ΔT with $\Delta\phi = 0°$, $\Delta\phi = 60°$, and $\Delta\phi = 120°$ progressively decrease, consistent with the above explanation. The 2×2 array in phase can cause a higher peak ΔT than the 4×1 array because the outer elements in the 4×1 array have lower contributions to the ΔT around the center of the head model. As mentioned above, the peak ΔT induced by the dipole antenna is higher than that by the 4×1 array for small h because the radiated power of the dipole is concentrated in a much smaller space at a very close distance. For the same reason, the peak ΔT induced by the 4×1 array is higher than that by the 8×1 array. For large h, the peak ΔT induced by the 8×1 array descents slower (and should be higher, in this study, $h > 20$ mm) than the peak ΔT induced by the 4×1, because in the far field, the peak ΔT is determined by the antenna gain.

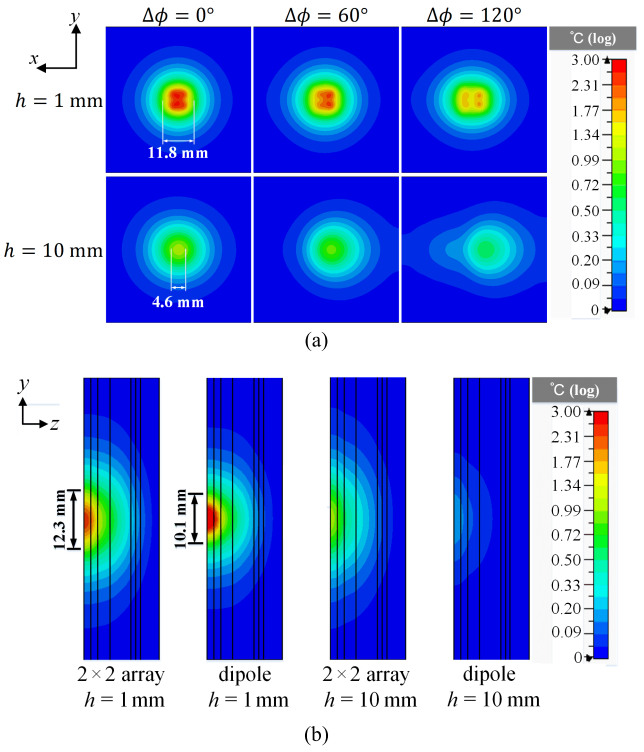

FIGURE 7. (a) ΔT distribution on the skin surface induced by the 2 × 2 patch array for $\Delta\phi = 0°$, 60°, and 120°. (b) plane cut of ΔT distribution in the *yz*-plane for the 2 × 2 patch array ($\Delta\phi = 0°$) and the single dipole with $h = 1$ mm and 10 mm. The dimension markings in the figures denote the size of the hot spot area higher than 1 °C.

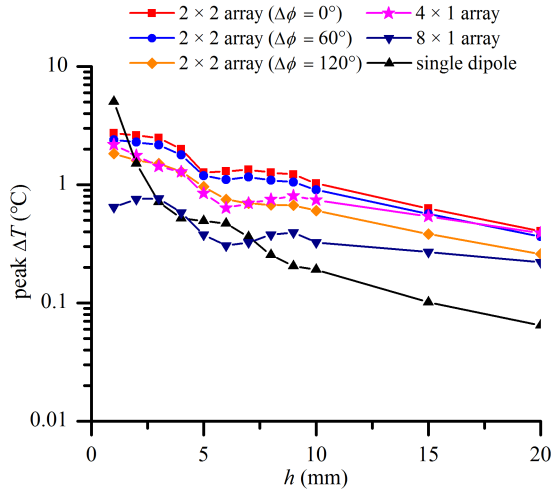

FIGURE 8. Peak ΔT versus h for different antennas.

D. CORRELATION BETWEEN TEMPERATURE ELEVATION AND INCIDENT POWER DENSITY

Incident power densities, denoted as S^{P} (the spatial-peak value), S^1 (averaged over 1 cm^2), S^{20} (averaged over 20 cm^2), and S^{114} (averaged over 114 cm^2 for the IEEE), are calculated using (5) and (7). The power density values are calculated with varying h for the correlations between the power density metrics in free space and the peak ΔT in the tissue. Using the peak ΔT values calculated in Fig. 8, the peak-ΔT-versus-power-density points for all the varying h from 1 mm to 20 mm are plotted in Fig. 9. The dashed lines are the linear fittings with intercept equal to zero for all peak-ΔT-versus-power-density markers except for the marker pointed out with the arrow, which is the extreme situation for the dipole at $h = 1$ mm. It shows that S^{P} and S^1 have a better linear correlation with the peak ΔT than S^{20} and S^{114}. This may be attributed to the fact that 20 cm^2 and 114 cm^2 are too large with respect to the footprint of mmWave antennas [38]. In the near field, the energy is mainly focused in a small portion of the area much smaller than 20 cm^2, thus in nature S^{20} and S^{114} have weaker correlation with the peak ΔT compared with S^{P} and S^1. The solid lines are calculated using uniform plane waves independent of the size of the averaging area, thus they are the same in Fig. 9(a)–Fig. 9(d). S^1 has a better agreement with plane-wave results than S^{P}, S^{20}, and S^{114}.

IV. DISCUSSION

The multi-layer model of human heads used in this study is similar to those used in [37] and [38], with a much smaller width and length (in comparison, the length and the width of the models used in [37] and [38] is 200 mm). In this study, the width and the length of the head model of 60 mm is large enough to achieve the convergent results for antennas operating closer than 20 mm. The ΔT induced by the dipole with 15 dBm input power at 28 GHz at $h = 20$ mm is about 0.1 °C, the same as the ΔT approximated by a Gaussian function in [39]. The heating factor defined in [38] as the ratio of the peak ΔT to the spatial-average power density is about 0.01 °C · m^2/W for plane waves at 28 GHz, which is equal to the slope of the solid line in Fig. 9. Our results are consistent with other literature, confirming the validity of our simulation settings.

Because 5G UE, such as smart phones and tablets, work very close to human bodies, it is meaningful to investigate near-field exposure scenarios. Because of the lack of wide deployment of mmWave devices before, the guidelines and standards neither give further instructions on how to evaluate power density near human bodies nor provide relevant rationale. Reference [28] claims that incident power density, as a free space dosimetric quantity, cannot directly indicate the thermal response as the SAR does in lower frequencies. In this study, however, the obtained results suggest that both S^{P} and S^1 have stable linear correlations with the peak ΔT for different antennas. S^1 also shows a good agreement with the plane waves.

For large averaging areas, [38] proposed a compensation factor to convert a non-uniform power density distribution to an equivalent radius. However, such a compensation factor requires prior knowledge of the SAR distribution, which depends on the separation distance and specific antennas, and such prior knowledge is hard to acquire in practice. Reference [11] suggested that the averaging area would be on the order of about 1–2 cm^2 provided by the Green's function solution to the BHTE, which agrees with our simulation

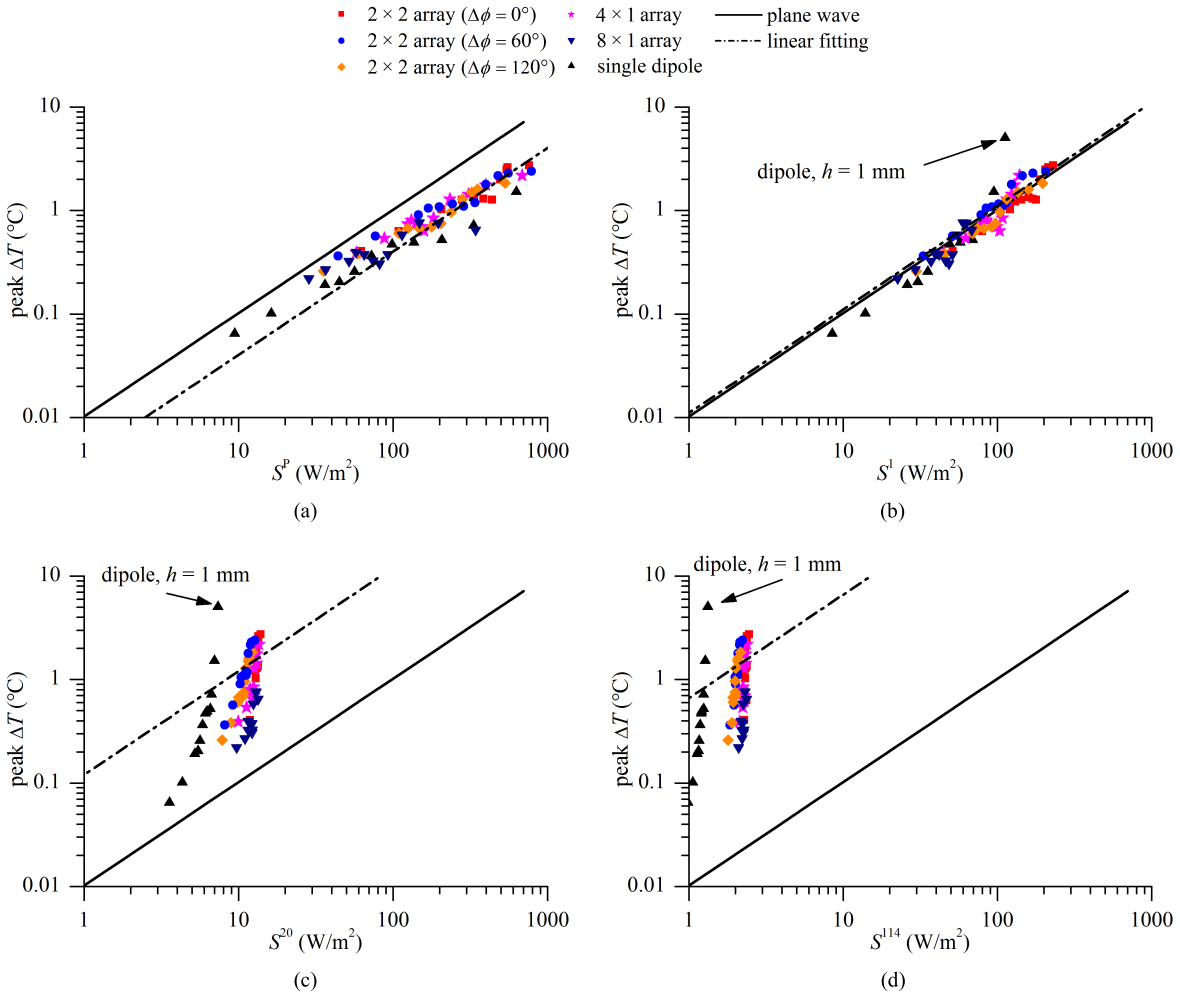

FIGURE 9. The relationship between the peak ΔT and the spatial-peak/spatial-average power density. Each marker represents each peak ΔT obtained in Fig. 8 for a certain h, versus the power density value obtained with the same h in free space. (a) peak ΔT versus S^{P}, (b) peak ΔT versus S^{1}, (c) peak ΔT versus S^{20} (d) peak ΔT versus S^{114}.

findings. Reference [38] suggested that the 4cm^2 averaging area determined from the plane-wave-beam exposure may be a better substitute for safety guidelines and standards. After all, the ongoing revision and updating of the safety guidelines and standards should consider the weakness of the uniform power density distribution and should consider the limited sizes of hot spots and the non-uniformity of power density distribution. The performance of the averaging area may depend on the frequencies, array configurations, and operating distances, thus further investigation and evidence would be needed.

The spatial-peak power density in the near field highly depends on the sample grid, computational algorithm error, and measurement error due to effects of probes, etc., thus more sensitive to simulation and measurement settings, while the spatial-average power density is more robust to these conditions.

The total transmitted power level of 15 dBm adopted in this paper is much lower than the transmitted power levels of current cellular UE (23–33 dBm). When $h < 4$ mm, the peak ΔT can be as high as 2–3 °C for 4-element arrays, while it is within 1 °C that the temperature elevation has no detrimental health effects [12], [13]. Manufacturers may need to use some kinds of designs to tune the transmitting beam away from human bodies to facilitate the mmWave transmission in 5G UE.

In this study, we assume the continuous wave signals to give a conservative estimate of ΔT, while in practice, considering the precoding methods and likely Time Division Duplexing (TDD), the steady state may take a longer period to reach, and a very high-date uplink rarely happens in practice [51], [52]. Such a case requires further investigation in laboratory measurements and field tests.

The thicknesses of the multi-layer model are the same as those in [37] and [38] (except for the brain, as the brain thickness has little impact on the peak ΔT,) so that the results are comparable. In practice, the thickness, thermal parameters, and dielectric parameters of each layer are variable [44]. Thus, uncertainty still exists to some extent, and the conclusions need further experimental verification.

V. CONCLUSION

In this study, we use BHTE and a multi-layer human head model to investigate the temperature elevation in tissues under the EMF exposure from antenna arrays around 28 GHz. Particularly, it shows that the maximum spatial-average power density with an averaging area of 1 cm^2 has a good correlation with the peak ΔT and a good agreement with the plane waves among the investigated metrics. The averaging area of a few square-centimeters may be a good candidate for the spatial-average power density. The findings and results on spatial-peak and spatial-average power density and their correlations with temperature elevation would be very useful input for the relevant safety standards and guidelines, mobile operators, and manufacturers.

ACKNOWLEDGEMENT

The authors thank Dr. Kun Zhao at KTH for his advice on the motivations of this study.

REFERENCES

[1] T. S. Rappaport *et al.*, "Millimeter wave mobile communications for 5G cellular: It will work!" *IEEE Access*, vol. 1, pp. 335–349, May 2013.

[2] J. G. Andrews *et al.*, "What will 5G be?" *IEEE J. Sel. Areas Commun.*, vol. 32, no. 6, pp. 1065–1082, Jun. 2014.

[3] A. Osseiran *et al.*, "Scenarios for 5G mobile and wireless communications: The vision of the METIS project," *IEEE Commun. Mag.*, vol. 52, no. 5, pp. 26–35, May 2014.

[4] C. A. Balanis, "Fundamental parameters of antennas," in *Antenna Theory: Analysis and Design*, 3rd ed. Hoboken, NJ, USA: Wiley, 2005, pp. 94–104.

[5] J. Wells, "Faster than fiber: The future of multi-G/s wireless," *IEEE Microw. Mag.*, vol. 10, no. 3, pp. 104–112, May 2009.

[6] W. Roh *et al.*, "Millimeter-wave beamforming as an enabling technology for 5G cellular communications: Theoretical feasibility and prototype results," *IEEE Commun. Mag.*, vol. 52, no. 2, pp. 106–113, Feb. 2014.

[7] J. Helander, K. Zhao, Z. Ying, and D. Sjöberg, "Performance analysis of millimeter-wave phased array antennas in cellular handsets," *IEEE Antennas Wireless Propag. Lett.*, vol. 15, pp. 504–507, Jul. 2015.

[8] N. Ojaroudiparchin, M. Shen, S. Zhang, and G. F. Pedersen, "A switchable 3-D-coverage-phased array antenna package for 5G mobile terminals," *IEEE Antennas Wireless Propag. Lett.*, vol. 15, pp. 1747–1750, 2016.

[9] I. Syrytsin, S. Zhang, G. Pedersen, K. Zhao, T. Bolin, and Z. Ying, "Statistical investigation of the user effects on mobile terminal antennas for 5G applications," *IEEE Trans. Antennas Propag.*, vol. 65, no. 12, pp. 6596–6605, Dec. 2017.

[10] S. Zhang, X. Chen, I. Syrytsin, and G. F. Pedersen, "A planar switchable 3D-coverage phased array antenna and its user effects for 28 GHz mobile terminal applications," *IEEE Trans. Antennas Propag.*, vol. 65, no. 12, pp. 6413–6421, Dec. 2017.

[11] K. R. Foster, M. C. Ziskin, and Q. Balzano, "Thermal modeling for the next generation of radiofrequency exposure limits: Commentary," *Health Phys.*, vol. 113, no. 1, pp. 41–53, 2017.

[12] A. Ahlbom *et al.*, "Guidelines for limiting exposure to time-varying electric, magnetic, and electromagnetic fields (up to 300 GHz)," *Health Phys.*, vol. 74, no. 4, pp. 494–522, Apr. 1998.

[13] *IEEE Standard for Safety Levels with Respect to Human Exposure to Radio Frequency Electromagnetic Fields, 3kHz to 300 GHz*, IEEE Standard C95.1-2005, (Revision of IEEE Standard C95.1-1991), 2006.

[14] *IEEE Standard for Safety Levels with Respect to Human Exposure to Radio Frequency Electromagnetic Fields, 3 kHz to 300 GHz Amendment 1: Specifies Ceiling Limits for Induced and Contact Current, Clarifies Distinctions between Localized Exposure and Spatial Peak Power Density*, IEEE Standard C95.1a, 2010.

[15] *Radio Frequency Radiation Exposure Limits*, Code of Federal Regulation Title 47, Part 1.1310, Federal Communications Commission, Washington, DC, USA, 2017.

[16] N. Kuster and Q. Balzano, "Energy absorption mechanism by biological bodies in the near field of dipole antennas above 300 MHz," *IEEE Trans. Veh. Technol.*, vol. 41, no. 1, pp. 17–23, Feb. 1992.

[17] T. Schmid, O. Egger, and N. Kuster, "Automated E-field scanning system for dosimetric assessments," *IEEE Trans. Microw. Theory Techn.*, vol. 44, no. 1, pp. 105–113, Jan. 1996.

[18] Y. Okano, K. Ito, I. Ida, and M. Takahashi, "The SAR evaluation method by a combination of thermographic experiments and biological tissue-equivalent phantoms," *IEEE Trans. Microw. Theory Techn.*, vol. 48, no. 11, pp. 2094–2103, Nov. 2000.

[19] E. P. Khizhnyak and M. C. Ziskin, "Infrared thermography in experimental dosimetry of radio frequency and millimeter wavelength radiation exposure," in *Radio Frequency Radiation Dosimetry and Its Relationship to the Biological Effects of Electromagnetic Fields*. Dordrecht, The Netherlands: Springer, 2000, pp. 199–206.

[20] P. Vainikainen, J. Ollikainen, O. Kivekas, and I. Kelander, "Resonator-based analysis of the combination of mobile handset antenna and chassis," *IEEE Trans. Antennas Propag.*, vol. 50, no. 10, pp. 1433–1444, Oct. 2002.

[21] H. Kawai and K. Ito, "Simple evaluation method of estimating local average SAR," *IEEE Trans. Microw. Theory Techn.*, vol. 52, no. 8, pp. 2021–2029, Aug. 2004.

[22] O. Kivekas, J. Ollikainen, T. Lehtiniemi, and P. Vainikainen, "Bandwidth, SAR, and efficiency of internal mobile phone antennas," *IEEE Trans. Electromagn. Compat.*, vol. 46, no. 1, pp. 71–86, Feb. 2004.

[23] B. B. Beard *et al.*, "Comparisons of computed mobile phone induced SAR in the SAM phantom to that in anatomically correct models of the human head," *IEEE Trans. Electromagn. Compat.*, vol. 48, no. 2, pp. 397–407, May 2006.

[24] Z. Ying, "Antennas in cellular phones for mobile communications," *Proc. IEEE*, vol. 100, no. 7, pp. 2286–2296, Jul. 2012.

[25] S. Zhang, K. Zhao, Z. Ying, and S. He, "Adaptive quad-element multi-wideband antenna array for user-effective LTE MIMO mobile terminals," *IEEE Trans. Antennas Propag.*, vol. 61, no. 8, pp. 4275–4283, Aug. 2013.

[26] K. Zhao, S. Zhang, Z. Ying, T. Bolin, and S. He, "SAR study of different MIMO antenna designs for LTE application in smart mobile handsets," *IEEE Trans. Antennas Propag.*, vol. 61, no. 6, pp. 3270–3279, Jun. 2013.

[27] H. Li, A. Tsiaras, and B. K. Lau, "Analysis and estimation of MIMO-SAR for multi-antenna mobile handsets," *IEEE Trans. Antennas Propag.*, vol. 65, no. 3, pp. 1522–1527, Mar. 2017.

[28] T. Wu, T. S. Rappaport, and C. M. Collins, "Safe for generations to come: Considerations of safety for millimeter waves in wireless communications," *IEEE Microw. Mag.*, vol. 16, no. 2, pp. 65–84, Mar. 2015.

[29] D. Colombi, B. Thors, and C. Törnevik, "Implications of EMF exposure limits on output power levels for 5G devices above 6 GHz," *IEEE Antennas Wireless Propag. Lett.*, vol. 14, pp. 1247–1249, 2015.

[30] B. Thors, D. Colombi, Z. Ying, T. Bolin, and C. Törnevik, "Exposure to RF EMF from array antennas in 5G mobile communication equipment," *IEEE Access*, vol. 4, pp. 7469–7478, 2016.

[31] K. Zhao, Z. Ying, and S. He, "EMF exposure study concerning mmWave phased array in mobile devices for 5G communication," *IEEE Antennas Wireless Propag. Lett.*, vol. 15, pp. 1132–1135, 2016.

[32] B. Xu *et al.*, "Power density measurements at 15 GHz for RF EMF compliance assessments of 5G user equipment," *IEEE Trans. Antennas Propag.*, vol. 65, no. 12, pp. 6584–6595, Dec. 2017.

[33] B. Xu *et al.*, "Investigation of planar near-field measurement of millimeter-wave antenna for 5G application," in *Proc. Int. Symp. Antennas Propag. (ISAP)*, Okinawa, Japan, Oct. 2016, pp. 600–601.

[34] J. Li, S. Yan, Y. Liu, B. M. Hochwald, and J. M. Jin, "A high-order model for fast estimation of electromagnetic absorption induced by multiple transmitters in portable devices," *IEEE Trans. Antennas Propag.*, vol. 65, no. 12, pp. 6768–6778, Dec. 2017.

[35] K. R. Foster, M. C. Ziskin, and Q. Balzano, "Thermal response of human skin to microwave energy: A critical review," *Health Phys.*, vol. 111, no. 6, pp. 528–541, 2016.

[36] R. Morimoto, I. Laakso, V. D. Santis, and A. Hirata, "Relationship between peak spatial-averaged specific absorption rate and peak temperature elevation in human head in frequency range of 1–30 GHz," *Phys. Med. Biol.*, vol. 61, pp. 5406–5425, Jul. 2016.

[37] R. Morimoto, A. Hirata, I. Laakso, M. C. Ziskin, and K. R. Foster, "Time constants for temperature elevation in human models exposed to dipole antennas and beams in the frequency range from 1 to 30 GHz," *Phys. Med. Biol.*, vol. 62, pp. 1676–1699, Feb. 2017.

[38] Y. Hashimoto *et al.*, "On the averaging area for incident power density for human exposure limits at frequencies over 6 GHz," *Phys. Med. Biol.*, vol. 62, pp. 3124–3138, Mar. 2017.

[39] K. Foster and D. Colombi, "Thermal response of tissue to RF exposure from canonical dipoles at frequencies for future mobile communication systems," *Electron. Lett.*, vol. 53, no. 5, pp. 360–362, Mar. 2017.
[40] H. H. Pennes, "Analysis of tissue and arterial blood temperatures in the resting human forearm," *J. Appl. Physiol.*, vol. 1, no. 2, pp. 93–122, 1948.
[41] *Notice of Proposed Rulemaking*, document 15-135, FCC, Commission, Oct. 2015.
[42] *Further Notice of Proposed Rulemaking*, document 16-89, FCC, Commission, Jul. 2016.
[43] B. Xu, K. Zhao, S. He, and Z. Ying, "Understandings of maximum spatially-averaged power density in 5G RF EMF exposure study," in *Proc. Int. Workshop Antenna Technol., Small Antennas, Innov. Struct., Appl. (iWAT)*, Athens, Greece, Mar. 2017, pp. 115–117.
[44] A. Drossos, V. Santomaa, and N. Kuster, "The dependence of electromagnetic energy absorption upon human head tissue composition in the frequency range of 300–3000 MHz," *IEEE Trans. Microw. Theory Techn.*, vol. 48, no. 11, pp. 1988–1995, Nov. 2000.
[45] S. Gabriel, R. W. Lau, and C. Gabriel, "The dielectric properties of biological tissues: III. Parametric models for the dielectric spectrum of tissues," *Phys. Med. Biol.*, vol. 41, no. 11, pp. 2271–2293, 1996.
[46] A. Hirata and T. Shiozawa, "Correlation of maximum temperature increase and peak SAR in the human head due to handset antennas," *IEEE Trans. Microw. Theory Techn.*, vol. 5, no. 7, pp. 1834–1841, Jul. 2003.
[47] *UE Antenna Array Configuration for mmWave 28 GHz*, document R4-1704864, 3GPP, Sophia Antipolis, Valbonne, France, 2017.
[48] *Computer Simulation Technology*. Accessed: Oct. 6, 2017. [Online]. Available: https://www.cst.com
[49] D. Fiala, K. J. Lomas, and M. Stohrer, "Computer prediction of human thermoregulatory and temperature responses to a wide range of environmental conditions," *Int. J. Biometeorol.*, vol. 45, no. 3, pp. 143–159, 2001.
[50] A. Hirata *et al.*, "Computational verification of anesthesia effect on temperature variations in rabbit eyes exposed to 2.45 GHz microwave energy," *Bioelectromagnetics*, vol. 27, no. 8, pp. 602–612, 2006.
[51] E. Dahlman, S. Parkvall, J. Sköld, and P. Beming, *3G Evolution: HSPA and LTE for Mobile Broadband*, 2nd ed. San Diego, CA, USA: Academic, 2008.
[52] *3rd Generation Partnership Project; Technical Specification Group Radio Access Network; Evolved Universal Terrestrial Radio Access (E-UTRA); Physical Channels and Modulation (Release 14)*, 3GPP Standard TS 36.211 V14.2.0, 3GPP, Jun. 2017.

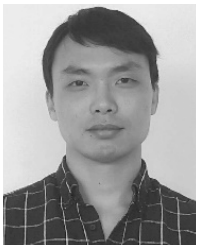

WANG HE received the B.E. degree in information engineering from Zhejiang University, Hangzhou, China, in 2015, where he is currently pursuing the Ph.D. degree with the Centre for Optical and Electromagnetic Research. His current research interests include antenna design, RFID technology, and RF EMF exposure.

BO XU (S'14) received the B.E. degree in information engineering from Zhejiang University, Hangzhou, China, in 2010. He is currently pursuing the joint Ph.D. degree with the Department of Electromagnetic Engineering, KTH Royal Institute of Technology, Stockholm, Sweden, and the Centre for Optical and Electromagnetic Research, Zhejiang University. He has been a visiting student with the Department of Electrical and Information Technology, Lund University, Lund, Sweden. His research interests include RF EMF exposure, mmWave antenna design, RFID, and antenna measurement.

MATS GUSTAFSSON (M'05–SM'17) received the M.Sc. degree in engineering physics and the Ph.D. degree in electromagnetic theory from Lund University, Sweden, in 1994 and 2000, respectively.

He was the Docent with Lund University in 2005, where he was a Professor of electromagnetic theory in 2011. He co-founded the company Phase Holographic Imaging AB in 2004. He has authored or co-authored over 65 peer-reviewed journal papers and over 85 conference papers. His research interests are in scattering and antenna theory and inverse scattering and imaging with applications in microwave tomography and digital holography.

Prof. Gustafsson received the Best Antenna Poster Prize at EuCAP 2007, the IEEE Schelkunoff Transactions Prize Paper Award 2010, and the Best Antenna Theory Paper Award at EuCAP 2013. He serves as an IEEE AP-S Distinguished Lecturer from 2013 to 2015.

ZHINONG YING (SM'05) joined Ericsson AB in 1995. He became a Senior Specialist in 1997 and an Expert in 2003 in his engineer career at Ericsson. He served as the TPC Co-Chairmen at the International Symposium on Antenna Technology (iWAT), in 2007, and served as a session organizer of several international conferences, including IEEE APS, and a reviewer for several academic journals. He has been a Guest Professor with the Joint Research Centre of KTH Royal Institute of Technology, Sweden, and Zhejiang University, China, since 2001. He is currently a Principle Engineer of antenna technology with the Network Technology Laboratory, Research and Technology, Sony Mobile Communications AB, Lund, Sweden, also as a Distinguish Engineer within the whole Sony group.

He has authored and co-authored over 140 papers in various journal, conference and industry publications. He holds more than 147 patents and pending in the antennas and new generation wireless network areas. His main research interests are small antennas, broad and multi-band antenna, multi-channel antenna (MIMO) system, antenna for body area network, antenna, and propagation in fifth generation mobile network, including massive MIMO and mmWave, near-field, and human body effects and measurement techniques. He contributed several book chapters on mobile antenna, small antenna and MIMO antennas in *Mobile Antenna Handbook* (Third Edition) edited by H. Fujimoto and the *Handbook of Antenna Technologies* edited by Z. N. Chen. He had contributed a lot of work in antenna designs and evaluation methods for the mobile industry. He has also been involved in the evaluation of Bluetooth technology which was invented by Ericsson. He was a member of Scientific Board of the Antenna Centre of Excellent in European 6th Frame Program from 2004 to 2007. He received the Best Invention Award at Ericsson Mobile in 1996 and the Key Performer Award at Sony Ericsson in 2002. He was nominated for the President Award at Sony Ericsson in 2004 for his innovative contributions. He received the Distinguish Engineer title at Sony Group globally in 2013.

SAILING HE (M'92–SM'98–F'13) received the Lic.Tech. degree and the Ph.D. degree in electromagnetic theory from the KTH Royal Institute of Technology, Stockholm, Sweden, in 1991 and 1992, respectively. Since then, he was with the KTH Royal Institute of Technology as an Assistant Professor, an Associate Professor, and a Full Professor. He also serves as the Director for a joint research center between the KTH Royal Institute of Technology and Zhejiang University, China. He has first-authored one monograph (Oxford University Press) and authored/co-authored about 500 papers in refereed international journals. His current research interests include applied electromagnetics, electromagnetic metamaterials, optoelectronics, microwave photonics, and biomedical applications. He has given many invited/plenary talks in international conferences, and has served in the leadership for many international conferences.